Author/s:
Vincent, CL;Larsén, XG;Larsen, SE;Sørensen, P

Title:
Cross-Spectra Over the Sea from Observations and Mesoscale Modelling

Date:
2013-02-01

Citation:
Vincent, C. L., Larsén, X. G., Larsen, S. E. & Sørensen, P. (2013). Cross-Spectra Over the Sea from Observations and Mesoscale Modelling. Boundary Layer Meteorology, 146 (2), pp.297-318. https://doi.org/10.1007/s10546-012-9754-1.

Noname manuscript No.
(will be inserted by the editor)

Cross-spectra over the sea from observations and mesoscale modelling

C L Vincent · X G Larsén · S Larsen · P Sørensen

Received: date / Accepted: date

Abstract Co-spectra and quadrature spectra are calculated for six pairs of tall offshore measurement masts near the Horns Rev I wind farm in the Danish North Sea and the Nysted wind farm in the Baltic sea. The mast-pairs are separated from one another by horizontal distances of 2.13 km to 12.4 km. Co-spectra and quadrature spectra for the two sites are classified in terms of the angle between the mean wind direction and the line connecting each pair of masts. The frequency axes of the spectra are normalized to remove the effect of mean wind speed and separation distance. Results indicate a larger contribution to the quadrature spectrum for flow from the sea than for flow from the land, and the patterns in the spectra are clearer and better defined

C. L. Vincent · X. G. Larsén · S. E. Larsen · P.Sørensen

Institut for Vindenergi - DTU Wind Energy

Tel.: +45 4677 5969

Fax: +45 4677 5083

E-mail: clav@dtu.dk

for Horns Rev I (which has a long uninterrupted sea-fetch from the west) than for Nysted (which is surrounded by a more complicated coast-line).

The analysis is replicated based on 3 month simulations using the weather research and forecasting (WRF) model with a horizontal grid spacing of 2 km. For the sea-fetch directions, good agreement in spectral properties between the model and observations is found. Analytical expressions based on the properties of the cross-correlation function and an exponentially decaying coherence function are fitted to the normalized co- and quadrature spectra. The expressions are shown to be a good fit to the spectra calculated from the WRF simulations and to the observed spectra for directions with a long sea fetch, which suggests that to a good approximation, the average co- and quadrature spectra over the sea can be written as functions of frequency, mean wind speed, separation distance and the angle between the wind direction and the orientation of the masts.

Keywords Cross-spectrum · Mesoscale modelling · Wind power fluctuations · Wind speed spectrum

1 Introduction

Successful implementation of high levels of wind energy within geographically limited areas such as the North Sea requires consideration of not only the mean wind and spectral properties of the wind at individual wind turbine locations, but also of the cross-spectral properties of the wind speed at multiple locations within a large wind farm or at multiple neighbouring wind farms.

This is because the aggregated power response of a number of turbines under fluctuating wind conditions depends on the extent to which fluctuations are correlated at individual turbine sites. This issue has been partly accounted for in wind farm power systems models such as those described in Sørensen et al (2002) and Vigueras-Rodrìguez et al (2010). Two different scenarios for the spatial distribution of wind fluctuations are illustrated in figure 1, where pairs of time series from two offshore meteorological masts near the Horns Rev I wind farm in the North Sea that are separated by a distance of 12.42 km are shown for 24 hour periods of longitudinal and lateral flow respectively. Here, longitudinal flow refers to flow where the mean wind direction is along the orientation of the two masts, and lateral flow refers to a mean wind direction perpendicular to the orientation of the masts. For the longitudinal case, there is an obvious lag between the time series, while for lateral flow case there is no obvious, systematic lag. In addition to differences caused by the systematic lag, the pairs of time series differ from one another due to the decay or development of eddies over the separation distance. Together, the co-spectrum and the quadrature spectrum quantify the contribution of in-phase and out-of-phase fluctuations to the overall covariance between pairs of time series as a function of frequency.

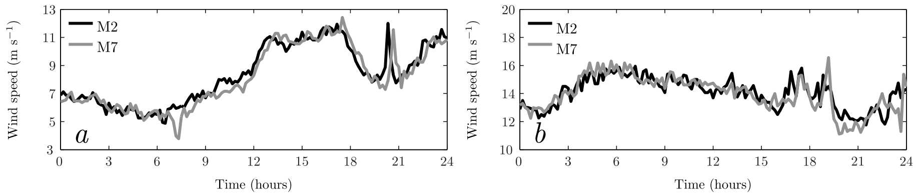

Fig. 1 Examples of pairs of wind speed observations from two masts near the Horns Rev I wind farm in the North Sea, separated by 12.42 km for longitudinal flow (a) and lateral flow (b)

The spectral properties of the wind speed and other atmospheric variables in the mesoscale range have been documented using a variety of data sets and analysis techniques. For example, Gage and Nastrom (1986) used measurements from commercial aircraft to calculate spectra in wave-number space, and established that when plotted on a log-log axes, the zonal and meridional wind components and temperature followed a spectral slope of $-5/3$ in the mesoscale range.

For length scales dominated by microscale fluctuations, the cross-spectral properties of pairs of wind speed observations have also been studied in detail. For example, Davenport (1961) calculated the coherence for pairs of vertically separated observations, and was the first to express the magnitude of the coherence, γ, as a function of vertical separation distance and a reference mean wind speed.

$$|\gamma| = \frac{|Co_{12}(f) + iQu_{12}(f)|}{\sqrt{(P_1(f)P_2(f)}} = e^{-k\frac{f}{V_0}\Delta z}, \quad (1)$$

where $Co_{12}(f)$ and $Qu_{12}(f)$ are the real and imaginary parts of the cross-spectrum between the two time series, P_1 and P_2 are the power spectra of the two time series, k is a decay constant, Δz is the vertical separation of the two observations and V_0 is a reference velocity near the ground. Kristensen (1979) derived expressions for the longitudinal coherence in the inertial sub-range by considering the loss of coherence due to lateral diffusion and Kristensen and Jensen (1979) presented theoretical and experimental results for the lateral coherence of the lateral and longitudinal wind components. In both cases, the expressions were based on the exponential decay of the coherence, and results were presented as a function of the dimensionless frequency $\frac{fd}{V_0}$, where d was a separation distance between the observations. These results were based on separation distances of a few tens of metres. Schlez and Infield (1998) combined expressions for lateral and longitudinal coherence to formulate empirical expressions for the coherence as a function of mean wind speed, separation distance and the angle between the mean wind direction and the orientation of pairs of masts for separation distances of 62–102 m. The decay factor in their expressions depended on the standard deviation of wind speed for lateral flow, and on standard deviation and mean wind speed for longitudinal flow.

Calculating cross-spectra for longer separation distances up to a few kilometres is, however, more problematic due to the challenges in obtaining suitable pairs of observations, particularly over the sea. Furthermore, for cross-spectra calculated for micro-scales one can easily find segments of time series for which stationarity is a good assumption. In contrast, cross-spectra based on separation distances of several kilometres correspond to time scales on which the atmosphere can rarely be treated as stationary. Sørensen et al (2002) used an expression for exponential decay of coherence together with decaying sine and cosine terms to express the complex coherence for separation distances of around 1 km for the purpose of wind energy power production modelling over the sea. Sørensen et al (2008) used a similar approach, but updated the decay parameters of Schlez and Infield (1998) using observational evidence from tall meteorological masts separated by 300–1200 m at a coastal site in Denmark. Nanahara et al (2004) calculated decay factors for separation distances between 100 m and 1700 m for flat and complex terrain sites. While they did not normalize the spectra by wind speed and separation distance, they also found that the decay factors were strongly dependent on the relative direction between the wind and the orientation of the masts. Woods et al (2011) built on expressions similar to those of Schlez and Infield (1998) to propose models for the co-spectrum and quadrature spectrum based on an extensive data set of pairs of measurement masts separated by distances of 1–30 km in south-eastern Australia. Their expressions were more complex than those of Sørensen et al (2002) and Schlez and Infield (1998) and include several extra fitted parameters. Larsén et al (2011b) calculated power spectra, co-spectra, quadrature spectra and coherences for pairs of tall meteorological masts over the North Sea and the Baltic Sea for different seasons and stability classes, and in the presence of open cellular convection and gravity waves. While they found little dependence of the average spectra on the surface layer stability itself, they showed that the presence of gravity waves in stable conditions and open cellular convection in unstable conditions (both of which introduce spatial variability on the scale of km) has a pronounced effect on the spectra.

In this work, the co-spectra and quadrature spectra over the sea are studied from three different perspectives. Firstly, normalized co-spectra and quadrature spectra are calculated using data from six offshore measurement masts: three over the North Sea near the Horns Rev I wind farm, and three over the Baltic Sea near the Nysted wind farm. The two sets of masts provide six mast-pairs with separation distances ranging from 2.13–12.42 km. All data has a measurement resolution of 10 min, and our time scales of interest are 20 min to 24 hr. Secondly, the analysis is replicated using mesoscale model simulations, where the focus is on conditions over the sea. Finally, mathematical models similar to those used by Sørensen et al (2002) are fitted to the normalized co-spectra and quadrature spectra from the mesoscale model, and it is implied that over the sea, the average spectra can be expressed as functions of frequency, wind speed, separation distance and angle between the mean wind direction and the orientation of the masts. The paper provides a methodology for the calculation of more accurate input to wind farm power system models such as that of Sørensen et al (2002), which rely on information about the spectral and co-spectral properties of the wind speed to calculate the power response of large wind farms or groups of wind farms. In particular, the results indicate that mesoscale modelling can be used to provide reasonable estimates of the co-spectrum and quadrature spectrum over the sea in cases where suitable observations are not available.

In section 2, the background to the normalized co-spectrum and quadrature spectrum is briefly outlined, and the formulation of an analytical model based on the Davenport equation and the properties of the complex cross spectrum, as applied by Sørensen et al (2002), is described. In sections 3 and 4, the observation data sets and mesoscale model simulations that were used in the analysis are described. In section 5, the normalized co-spectra and quadrature spectra based on observations and mesoscale modelling are presented, together with the proposed semi-empirical functions that relate the shape of the spectra to the wind direction, separation distance and relative angle of the mean wind to the orientation of the mast-pairs. Discussion and concluding remarks are given in sections 6 and 7 respectively.

2 The co-spectrum and quadrature spectrum

The co-spectrum and quadrature spectrum are the real and imaginary parts respectively of the complex cross-spectrum. When normalized by the power spectra of the two input time series, the normalized co-spectrum and quadrature spectrum make up the real and imaginary parts of the coherence, Coh, which is often expressed as an absolute value, $\gamma = |Coh|$.

$$\gamma(f) = \frac{|\overline{C_{12}}(f)|}{\sqrt{\overline{P_1(f)P_2(f)}}}, \quad \text{or,} \tag{2}$$

$$\gamma(f) = \frac{|\overline{Co_{12}}(f) + i\overline{Qu_{12}}(f)|}{\sqrt{\overline{P_1(f)P_2(f)}}}, \tag{3}$$

where C_{12} is the complex cross spectrum of two time series, P_1 and P_2 are the power spectra of the time series, and Co_{12} and Qu_{12} are the co-spectrum and quadrature spectrum. In this paper we work with the normalized co-spectrum and quadrature spectrum, $\mathrm{Co_n}$ and $\mathrm{Qu_n}$, and the complex coherence, Coh:

$$\mathrm{Co_n}(f) = \frac{\overline{Co_{12}}(f)}{\sqrt{\overline{P_1(f)P_2(f)}}} \tag{4}$$

$$\mathrm{Qu_n}(f) = \frac{\overline{Qu_{12}}(f)}{\sqrt{\overline{P_1(f)P_2(f)}}} \tag{5}$$

$$\mathrm{Coh}(f) = Co_n(f) + i\mathrm{Qu_n}(f) \tag{6}$$

Together, the normalized co-spectrum and the normalized quadrature spectrum describe the in-phase and out-of-phase contributions to the covariance of the two time series. Time series that are perfectly correlated at a certain frequency have a normalized co-spectrum of one and a normalized quadrature spectrum of zero at that frequency, while identical time series with a half-cycle phase-shift have a normalized co-spectrum of -1 and a normalized quadrature spectrum of zero. Time series that are one quarter cycle out-of-phase have a normalized co-spectrum of zero and a normalized quadrature spectrum of ±1, depending on whether the first time series leads or lags the second.

If the coherence is calculated for a single pair of time series, then it will be identically equal to unity for all frequencies, since $|C_{12}(f)| \equiv |\mathcal{F}_1(f)\mathcal{F}_2^*(f)|$, where $\mathcal{F}$ denotes a Fourier transform, which is identical to the denominator of the coherence. On the other hand, if the time series is divided into N segments, and the numerator and denominator are both calculated for each segment and averaged, then the correct formulation of the coherence is obtained. As discussed by Kristensen and Kirkegaard (1986), this procedure is problematic for many time series from the geophysical sciences, since the time series are usually non-stationary and not available for sufficient time periods for the calculation of meaningful averages. This is a particular problem for the analysis of mesoscale coherence, where we generally have no more than 24 hr periods of even near-stationary conditions, and any subdivision of the available time series into shorter segments results in an impractical loss of data at low frequencies. A solution is proposed by Kristensen and Kirkegaard (1986), who show that the coherence calculated from a block averaged (smoothed) single realization of the spectra and cross-spectra is equivalent to averaging over a large number of segments. Analysis using the two methodologies suggests that the resultant co-spectra and quadrature spectra are relatively insensitive to the choice of analysis methodology, and to the degree of smoothing that is applied in the block averaging.

For pairs of time series with systematic lag between them, such as pairs of wind speed observations separated in the longitudinal direction, there will be an offset in the maximum of the cross-covariance function, which introduces a bias into the cross-spectrum (Madsen, 2008). Specifically, it appears as non-zero values in the quadrature spectrum. Removing the lag by adjusting the time series for the effect of advection means that the quadrature spectrum will be near-zero for most frequencies. On the other hand, apparently systematic phase differences between pairs of meteorological time series are never likely to be as simple as pure advection. On time scales such as the diurnal cycle, time series from masts separated by tens of kilometres will be perfectly in phase, while we expect a transition to phase differences dominated by advection for time scales of several hours. Furthermore, advection is not the only physical process responsible for the movement of mesoscale features, as evident by the steering of convective systems by wind well above the surface (eg. Sioutas and Flocas (1996)), anomalous propagation of severe thunderstorms (eg. Davies-Jones (2002)) or gravity waves (Larsén et al, 2011a). For these reasons, we choose not to adjust the lag in the pairs of wind speed time series.

Sørensen et al (2002) proposes writing the cross-spectrum as:

$$C(f) = \gamma\sqrt{P_1(f)P_2(f)}e^{2\pi f\tau_{12}i}, \tag{7}$$

where γ is the magnitude of the coherence, f is the frequency and τ_{12} is the delay time, which in this model is assumed to be dominated by advection and is therefore constant. The normalized complex cross spectrum (Coh) can then be written as:

$$Coh(f) = \gamma e^{2\pi f\tau_{12}i} \tag{8}$$

Following the format of Davenport (1961), the magnitude of Coh can be expressed in the form $e^{a\frac{fd}{V_0}}$, where d is a separation distance, f is the frequency, a is a constant and V_0 is the mean wind speed over the time series under consideration, so the complex coherence becomes

$$Coh(f) = e^{(adf/V_0)} e^{-2\pi f \tau_{12} i}. \tag{9}$$

By consideration of advection between the two points, the delay time can be written as

$$\tau_{12} = \frac{dcos(\alpha)}{V_0}, \tag{10}$$

where α is the angle between the mean wind speed and the line connecting the two points and $dcos(\alpha)$ is the separation distance along the mean wind direction. Combining equations 9 and 10 gives

$$Coh(f) = e^{(-adf/V_0)} e^{-2\pi f \frac{cos(\alpha)d}{V_0} i} \tag{11}$$

Equation 11 can be simplified by defining a dimensionless frequency, $n = \frac{fd}{V_0}$, which adjusts for differences in the spectra due purely to different advection rates. Using the normalized frequency, equation 11 becomes

$$Coh(n) = e^{an} e^{bni}, \tag{12}$$

where a is an unknown constant and $b = -2\pi cos(\alpha)$.

Taking the logarithm of both sides, and equating real and imaginary parts shows that the constants a and b can be found empirically from the slope of the real and imaginary parts respectively of the log of the complex coherence.

$$\log(Coh(n)) = an + bni \tag{13}$$

$$\Re(\log(Coh(n))) = an \tag{14a}$$

$$\Im(\log(Coh(n))) = bn \tag{14b}$$

The normalized co-spectra and quadrature spectra are then written as:

$$\mathrm{Co_n} = e^{an} cos(bn) \tag{15a}$$

$$\mathrm{Qu_n} = e^{an} sin(bn) \tag{15b}$$

In section 5.3 of this paper, the parametrization in equations 15a and 15b is used to fit curves to the normalized co-spectrum and quadrature spectrum calculated from WRF simulations. It is shown that the parameters a and b both vary sinusoidally with the angle α, allowing $\mathrm{Co_n}$ and $\mathrm{Qu_n}$ to be written as functions of α, separation distance d and mean wind speed V_0.

3 Observation data

The calculation of mesoscale co-spectra and quadrature spectra over the sea requires pairs of observations from offshore measurement masts separated by distances of several kilometres up to tens of kilometres. The offshore measurement masts installed in association with the Horns Rev I and Nysted offshore wind farms satisfy these requirements, and provide a unique opportunity for calculating mesoscale co-spectra and quadrature spectra. At each site, three tall measurement masts operated continuously during the early stages of the wind farms' operations. There are three mast-pairs for each site, separated by varying distances and aligned along various orientations (Table 1). Measurements of wind speed and direction were available at several heights for each mast. We focus on top-mounted wind speed observations, thereby avoiding difficulties associated with boom distortion at lower levels.

Table 1 Mast pairs at the Horns Rev I and Nysted wind farms. The orientation refers to the wind direction that would blow from the first to the second mast in the pair.

Mast	Separation distance (km)	Orientation	Measurement period	Measurement heights (m)
Horns Rev M2-M6	8.72	295°	2003–2006	62 / 70
Horns Rev M2-M7	12.42	287°	2003–2006	62 / 70
Horns Rev M6-M7	3.99	269°	2003–2006	70 / 70
Nysted M1-M2	2.13	343°	2004–2008	69 / 69
Nysted M2-M3	8.90	280°	2004–2008	69 / 69
Nysted M1-M3	8.18	273°	2004–2008	69 / 69

Although the masts are offshore, the flow was influenced by the nearby land as well as the wind farm wakes. In figure 2, the positions of the masts in relation to the turbines and the undisturbed flow from the sea sectors are is shown.

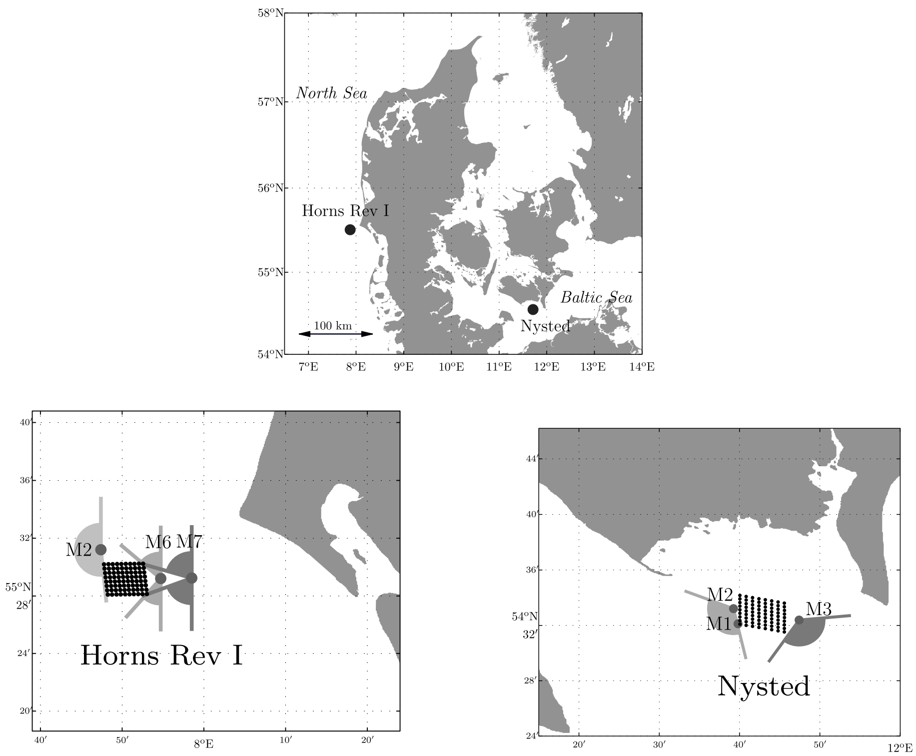

Fig. 2 The locations of the Horns Rev I and Nysted wind farms (top), and the meteorological masts (grey dots) and turbine locations (black dots) at the two sites (lower panels). The undisturbed flow sectors for the two sites are indicated by the shaded arcs.

For calculation of co-spectra and quadrature spectra over the sea, it is preferable that both masts are free from wake and land effects. This restrictive condition means that it is necessary to discard most of the data, and in particular it becomes nearly impossible to calculate spectra for longitudinal flow between the masts due to the turbines located between the masts. Therefore, these conditions were relaxed, and all directions were included in the analysis. In fact, the wind farm wake may not actually influence the spectra on the time scales that we are interested in, since Larsen et al (2009) has shown that the wind speed in the wake of an 80-m diameter turbine rotor contains enhanced variance only for frequencies greater than about 0.004 Hz and Sørensen et al (2008) noted increased turbulence in wake affected wind speeds for frequencies greater than about 0.001 Hz. The interaction of wakes from multiple turbines is complicated, and as discussed by Troldborg et al (2011), dependent on ambient turbulence. On the other hand, Larsén et al (2011b) calculated cross-spectra and quadrature spectra using only data that was free of wake effects, and the results are highly consistent with those in the current paper, which suggests that the wake effects may not be significant. Furthermore, the power spectra at all three masts are similar to one another and follow expected spectral shapes, including masts 6 and 7 at Horns Rev which are often in the wake of the whole wind farm due to the prevailing westerly winds, indicating no strong influence of the wake for our frequencies of interest.

Pairs of time series were analyzed in 24 hour segments, each consisting of 144 ten minute observations. Due to missing data and large changes in meteorological conditions during some periods, it was necessary to reject many of the 24 hour segments. Although meteorological time series are never strictly stationary, a compromise between including sufficient data in the analysis and choosing the best possible time series for the analysis was sought. The following segments were therefore rejected from the analysis: segments where more than one observation was missing from either of the two time series, segments where the average wind direction at the two sites differed by more than 15 degrees or the average wind speed differed by more than 2 m s^{-1} (indicating possible errors in one or both the data sets, since natural variability between the two sites is small), segments where the range of wind directions was greater than 90 degrees and segments where the range of wind speeds was more than 12 m s^{-1}. The single missing observation from some of the segments was filled by linear interpolation. Due to these restrictions, the mean of the time series, V_0, makes physical sense as an advection velocity under relatively homogeneous conditions, and the segments do not contain changes of air mass due to large direction changes. Furthermore, the calculation of spectra and co-spectra is only valid for stationary time series, and the restrictions are an attempt to use near-stationary time series for the analysis. After applying these criteria, 364, 371 and 476 segments remained for the mast pairs M2-M6, M2-M7 and M6-M7 at Horns Rev I respectively, and 305, 325 and 274 segments remained for the mast pairs M1-M2, M2-M3 and M1-M3 at Nysted respectively. These segments include both undisturbed flow from the sea, and land-influenced and wake-influenced flow.

4 Mesoscale simulations

For each region, a 90 day period was simulated using the WRF mesoscale model Version 3.3 (Skamarock et al, 2008). The North Sea simulation ran for the period October–December 2004, and the Baltic Sea simulation ran for October–December 2006. The periods were chosen to match data for verification purposes, but since we deal with average spectra, the precise time periods of the model runs are not compared with equivalent time periods in observational data anyway. The months October–December are chosen to cover a range of atmospheric conditions, including the cold air-outbreak situations found during these months, which are expected to be important for mesoscale coherence due to organized boundary structures such as convective rolls or cellular convection.

The three-month simulation periods are in contrast to the observational time series of several years, and have the disadvantage that they do not represent a long enough time period to be considered as a climatological average. On the other hand, Larsén et al (2011b) suggests that average spectra in the range 10^{-5}–10^{-3} Hz are not very sensitive to the seasonal or yearly scales, although the relative occurrence of mesoscale phenomena at certain times of year could affect the analysis. Furthermore, the mesoscale model has the advantage that we are not restricted to fixed observational sites. Due to the gridded nature of the model output, it is always possible to find pairs of points which are almost upwind of one another, or pairs that are aligned in an almost cross-wind direction. This meant that it was possible to use every 24 hour period that satisfied the basic stationarity criteria described in section 3 for any direction of interest, so no additional subdivision into direction sectors was necessary.

After filtering for stationarity, 36 days remained for the North Sea, and 60 days remained for the Baltic Sea.

The WRF simulations used data from the National Centers for Environmental Prediction Climate Forecast System Reanalysis[1] for initial and boundary conditions. Simulations ran in blocks of 11 days, with the first 24 hours discarded for spin-up purposes. Nudging was applied to the outer domain to keep the simulations close to the realistic evolution of the large scale weather. The model had 37 vertical levels, with the lowest five positioned close to 14 m, 52 m, 103 m, 160 m and 224 m, and three nests with horizontal grid spacings of 18km, 6km and 2km (figure 3).

The boundary layer parametrization was the MYNN scheme (Nakanishi and Niino, 2009), and the two larger domains used the Kain-Fritsch cumulus parametrization (Kain and Fritsch, 1990), while for the smallest domain the cumulus parametrization was turned off. It is expected that for a horizontal grid spacing of less than about 5 km, the effect of cumulus convection will be at least partly resolved (Molinari and Dudek, 1992), and we expect that explicit cumulus processes could make a significant contribution to mesoscale fluctuations and their spatial correlation.

[1] U.S. National Centers for Environmental Prediction [Environmental Modeling Center], 2010: NCEP Climate Forecast System Reanalysis (CFSR) Selected Hourly Time-Series Products, January 1979 to December 2010. Dataset ds093.1 published by the CISL Data Support Section at the National Center for Atmospheric Research, Boulder, CO, available online at http://dss.ucar.edu/datasets/ds093.1/.

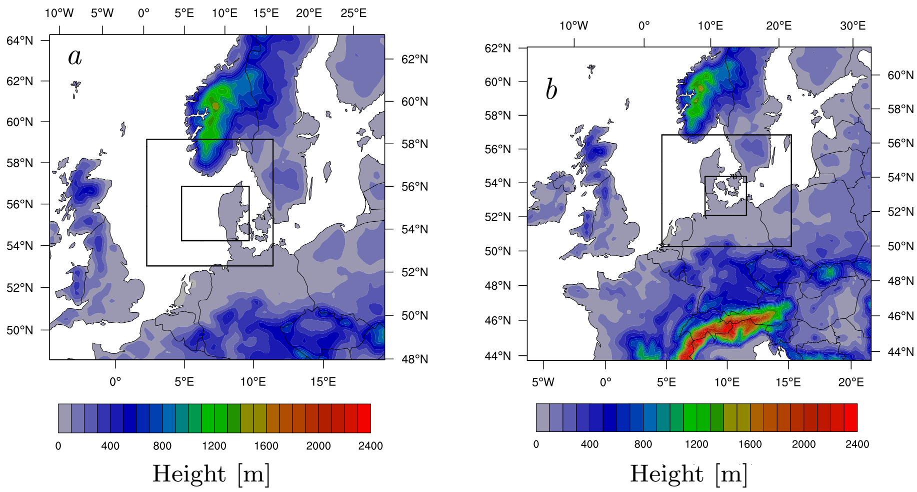

Fig. 3 WRF simulation domains for the North Sea (a) and the Baltic Sea (b).

For calculation of cross-spectra equivalent to those from the observational data, the wind components for the lowest five model levels were saved every 10 minutes. Model output from the third model level at a height of about 103 m was used for the analysis. When compared with observed wind speeds, the simulations had correlation coefficients of 0.90 at Horns Rev M7 and 0.91 at Nystedk, although it is the spatial variability and not the absolute values of the model that are of primary consideration here, and we did not correct for the difference between the model level and the measurement heights. To assess whether the fast variations in wind speed are modelled correctly, spectra of the modelled time series are compared with observed spectra for the meteorological masts at Horns Rev I and Nysted (figure 4). The spectral slope is well modelled up to the highest resolvable time period of 20 minutes. Both the observed and the model spectra follow a spectral slope of -3 for time scales longer than about

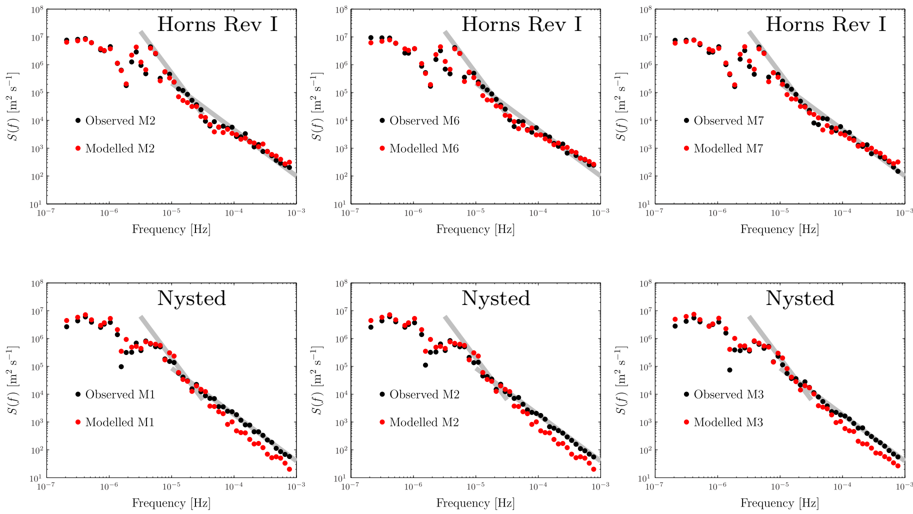

Fig. 4 Observed and modelled spectra of wind speed at Horns Rev I M2, M6 and M7 and Nysted M1, M2 and M3 respectively for the 90 day climate runs. The observations are at the heights described in table 1. The modelled wind speeds are from the third model level at a height of about 103 m. The thick grey lines indicate a spectral slope of -3 (periods greater than 24 hours) and $-5/3$ (periods less than 24 hours).

24 hours, and a spectral slope close to $-5/3$ for shorter time scales, following observational evidence of Nastrom and Gage (1985).

5 Results

As discussed in section 2, the frequency axes of the co-spectra and quadrature spectra were normalized by $\frac{V_0}{d}$, where V_0 is the mean wind speed and d is the separation distance, to give a non-dimensional frequency. The normalization of the frequency axis for longitudinal flow from the sea for the three pairs of meteorological masts at Horns Rev I is demonstrated in figure 5. The normalization causes the spectra to collapse onto a single curve, thereby removing

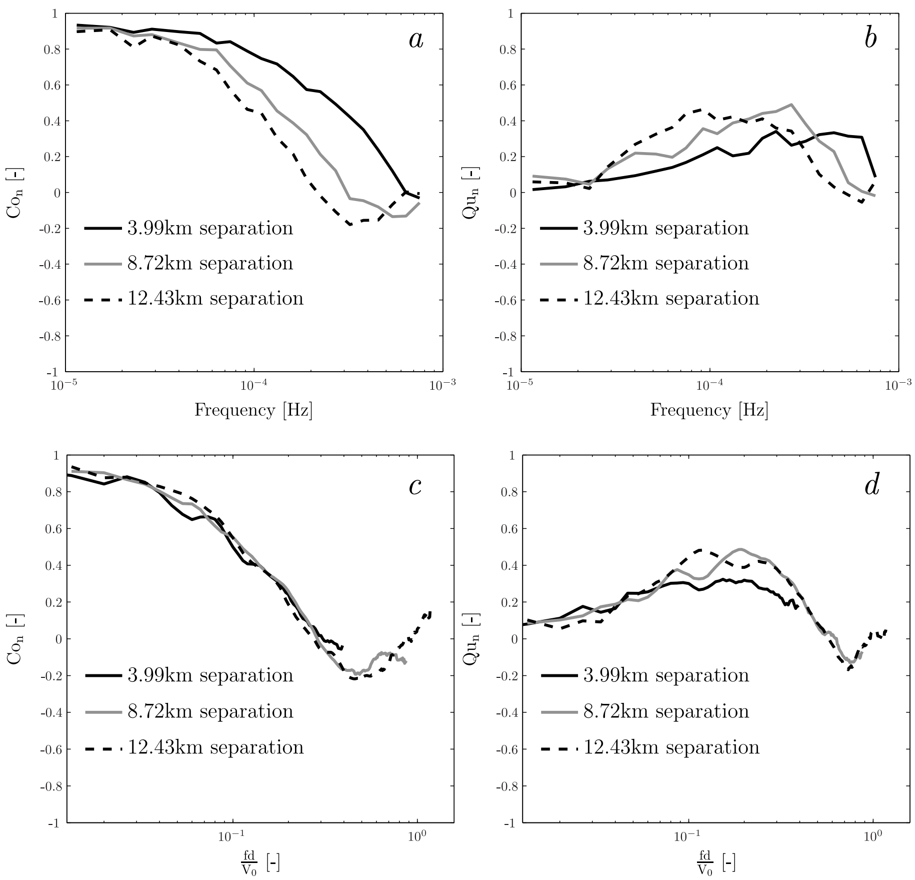

Fig. 5 Co-spectra (a and c) and quadrature spectra (b and d) of wind speed as a function of frequency (a and b) and normalized frequency (c and d) for the three mast-pairs at Horns Rev I for longitudinal flow from the sea.

the impact of wind speed and separation distance. The normalized frequency will be used for subsequent spectra in this paper.

5.1 Observed normalized co-spectra and quadrature spectra as functions of α

The 24 hour segments that satisfied the stationarity criteria were grouped into 8 direction bins according to the mean wind direction during the segment. Since the cases had already been selected on the basis that the range of wind directions was not more than 90^o, the average wind direction was sufficient to further classify the cases. The direction bins each had width 45^o, and were defined with respect to the direction of the line separating the two masts such that the angle α was 0^o, 45^o, 90^o, 135^o, 180^o, 225^o, 270^o and 315^o at the centres of the eight bins. This means that the first and fifth bins are both cases where the mast separation is longitudinal, but in opposite directions. Similarly the third and seventh bins are cases of lateral separation. The number of cases in the bins ranged between 9 and 89 for Horns Rev I and between 9 and 92 for Nysted. 9 cases is not large enough to form a representative sample, but all bins are retained for completeness.

Figure 6 shows co- and quadrature spectra for the eight direction sectors for Horns Rev I M2 and M7 (separation 12.43 km) and Nysted M1 and M3 (separation 8.13 km). It is important to realize that the directions labelled on the graphs are α (the angle between the wind direction and the separation of the masts), not the mean wind direction. Due to the orientation of the masts in a nearly east-west direction at Horns Rev I, $\alpha = 0^o$ corresponds nearly to easterly wind directions and $\alpha = 180^o$ corresponds nearly to westerly wind directions. Most direction sectors are influenced by the wind farm wake, the land or both. In this analysis, all directions have been included, but the only sector that is completely uninfluenced by the land or the wake is $\alpha = 45^{o}$. At Nysted, $\alpha = 90^{o}$ corresponds nearly to northerly flow from the land, while $\alpha = 270^{o}$ corresponds nearly to southerly flow from the sea. All directions will be influenced by wind farm wake or the land or both.

The normalized co-spectra are similar for each of the 8 direction bins, while the normalized quadrature spectra are strongly dependent on α. For the longitudinal cases, where there will be a maximum lag or lead between the two time series as a result of advection between the masts, the quadrature spectra reach a peak of around 0.4 for the westerly direction and -0.3 for the easterly direction at Horns Rev I. The difference in the magnitude of the longitudinal quadrature spectra may be because in easterly flow, the Horns Rev I wind farm is influenced by the land, 11 km to the east of the wind farm.

At Nysted, the quadrature spectrum has a peak of around 0.4 for the westerly sector, but does not follow any obvious pattern for the easterly sector. This may reflect an effect of the coast line, the fact that there are only 17 cases for this sector, or the different meteorological conditions over the Baltic Sea as compared with the North Sea. Similarly, the normalized co-spectrum dips further below zero to -0.22 at Horns Rev I for longitudinal flow from the sea, while the Nysted spectra appear to level off to zero for all direction sectors for normalized frequencies greater than 0.25.

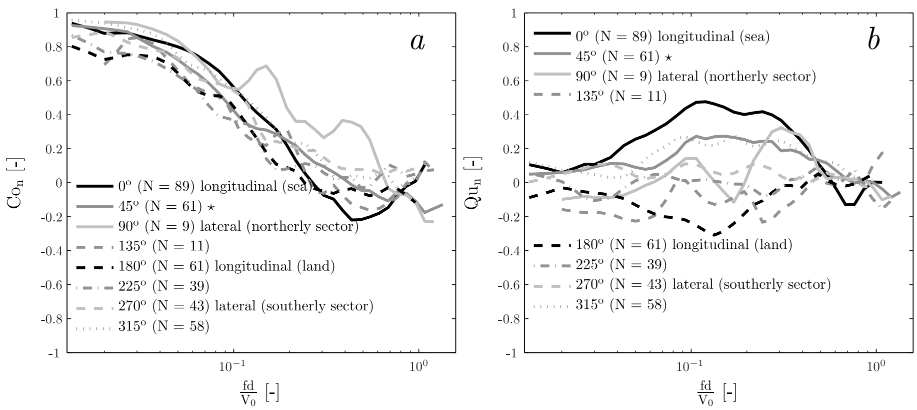

Fig. 6 Normalized co-spectra (a) and quadrature spectra (b) of wind speed for 8 different direction sectors for the M2–M7 pair at Horns Rev I. The separation distances is 12.43 km. The star indicates the only direction sector that is completely free from the influence of the wind farm wake or the land. The number of 24-hour periods included in each direction sector is indicated in brackets in the figure legends.

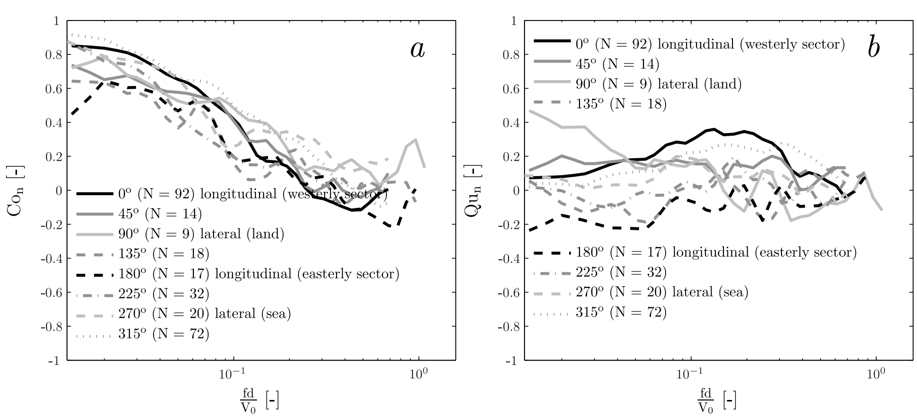

Fig. 7 Normalized co-spectra (a) and quadrature spectra (b) of wind speed for 8 different direction sectors for the M1–M3 pair at Nysted. The separation distances is 8.18 km. The number of 24-hour periods included in each direction sector is indicated in brackets in the figure legends.

5.2 Normalized co-spectra and quadrature spectra from WRF as functions of α

Calculation of co- and quadrature spectra from observations is complicated by the difficulties of data availability. For any direction of interest, there will only be a handful of 24 hour periods where the wind direction stays within a satisfactorily small range of the target direction. To obtain enough data for analysis, we are inevitably pushed to relax the conditions of stationarity and to consider a relatively wide window of wind directions.

Mesoscale modelling can alleviate some of these problems, because for any wind direction, it is easy to choose grid points that correspond to a given α and separation distance. Therefore, any 24 hour periods that satisfy the stationarity criteria can be used to study a range of wind directions and separation distances. On the other hand, mesoscale modelling is limited by its coarse resolution. Amongst other things, the parametrized vertical mixing in the boundary layer and the absence of explicit turbulent fluctuations and entrainment at the top of the boundary layer make it impossible to use mesoscale modelling to study micro-scale processes in the atmosphere. In this paper, however, we are concerned with cross-spectra for separation distances of several km. As demonstrated by Skamarock (2004), the WRF mesoscale model begins to lose spectral power for scales smaller than about 6-7 times the horizontal grid spacing of the model. This agrees with the model spectra for the 2 km simulation in figure 4, which show excellent agreement between the observations and model up to the time scale of 20 min, which for an average wind speed of around 10 m s^{-1} corresponds to a spatial scale of around 12 km. This suggests that it is indeed reasonable to use a model with a horizontal resolution of 2 km to study co- and cross-spectra for separation distances longer than about 12 km.

A reference point was chosen in each domain, and for each 24-hour period, the grid-points corresponding to an angle α and separation distance d were chosen in relation to the reference point, as illustrated in figure 8. The choice of grid-points corresponding to different values of α is dependent on the wind direction, and changes with each 24 hour period.

Unlike the co- and quadrature spectra calculated from observations, which were a mixture of easterly sector wind directions influenced by the nearby land, and westerly sector wind directions influenced by the sea, the WRF reference points were located slightly further out into the water so that both points had at least 10 km of sea fetch. Furthermore, we do not link a particular α value with a particular wind direction, since the grid points relating to a particular value of α varies as the mean wind direction varies. Therefore, systematic effects of the land or climatologically preferred weather regimes for certain values of α are less likely than for the observed spectra.

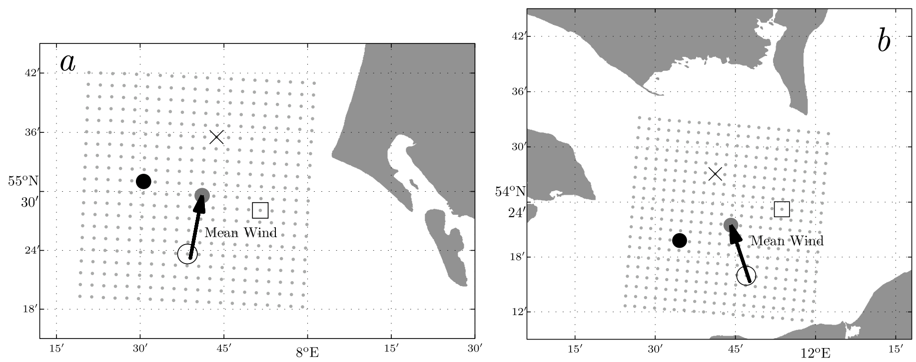

Fig. 8 The subset of domain 3 points used for the analysis (small grey dots). (*a*) North Sea near the Horns Rev I wind farm. (*b*) Baltic Sea near the Nysted wind farm. The large grey dot is the reference point, and the black arrow indicates mean wind direction. The grid points chosen for $\alpha = 0^{\circ}$, 90°, 180° and 270° are indicated by the symbols open circle, closed circle, cross and square respectively.

The co- and quadrature spectra calculated from the WRF simulations are shown in figure 9, using a 12 km separation distance between the pairs of points. The spectra show many features in common with the corresponding spectra from observations. The normalized co-spectra are not strongly dependent on α, while the quadrature spectra are close to zero for across-wind cases and reach the maximum amplitude for the along wind cases.

The clear patterns in the spectra from the mesoscale simulations allow an obvious interpretation of the positions of the local extrema and zero crossings. At very low normalized frequencies, the two time series are perfectly in phase, since they are both governed by exactly the same large scale and diurnal forcing. Clearly, the normalized co-spectrum must start at 1, and the quadrature spectrum must start at 0. For the frequency associated with eddies of size four times the separation distance, the time series at the two points are 90^{o} out of phase, and the quadrature spectrum is at its maximum value and the normalized co-spectrum is exactly equal to zero. In this case, the period of the fluctuations is $\frac{4d}{V_0}$, and the normalized frequency is 1/4. This is clearly seen on the plots - the extrema in the quadrature spectra match with the zero crossing in the normalized co-spectrum for a normalized frequency of 1/4. By similar reasoning, the minima in the longitudinal normalized co-spectra match with the zero crossing in the normalized quadrature spectra for a normalized frequency of 1/2, and the extrema in the longitudinal quadrature spectra match with the final zero crossing in the normalized co-spectra for a normalized frequency of 3/4.

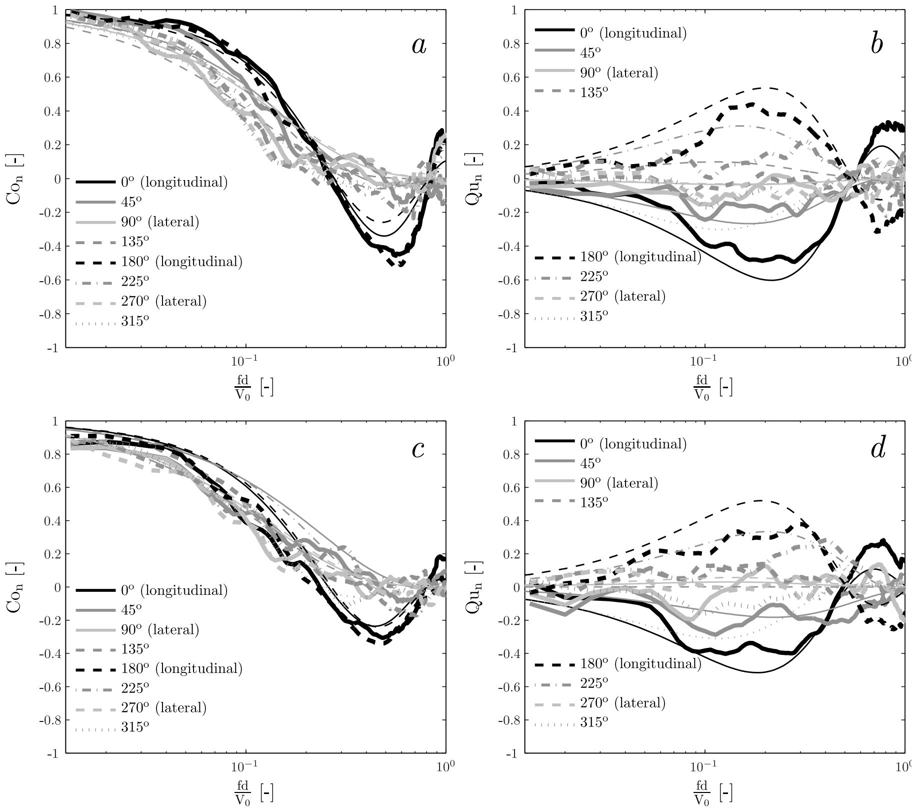

Fig. 9 Normalized co-spectra (a and c) and quadrature spectra (b and d) for wind speed for 8 different values of α based on WRF simulations over the North Sea (a and b) and the Baltic Sea (c and d). The separation distance is 12 km. Thick lines: Spectra calculated from WRF simulations. Thin lines: Fitted spectra using equations 15a and 15b.

5.3 Mathematical models for the normalized co- and quadrature spectra

In equations 15a and 15b, it was shown that the co- and quadrature spectra could be expressed as functions of the normalized frequency and two fitted parameters a and b. Furthermore, it was shown that the two parameters could be determined from the slope of the real and imaginary parts of the logarithm of the complex coherence when plotted against normalized frequency.

Figure 10 shows the parameters a and b as functions of the angle α, for separation distances 12–18 km, which suggests that both parameters vary with α but are invariant to separation distance. Both parameters can be modelled by sinusoidal functions, which means that the co- and quadrature spectra can be expressed as functions of only α and the normalized frequency, or alternatively as functions of α, wind speed, separation distance and frequency. The solid line shows a sinusoidal fit to the data for the parameter a. For parameter b, it was found that the theoretically derived $2\pi cos(\alpha)$ gave an excellent fit.

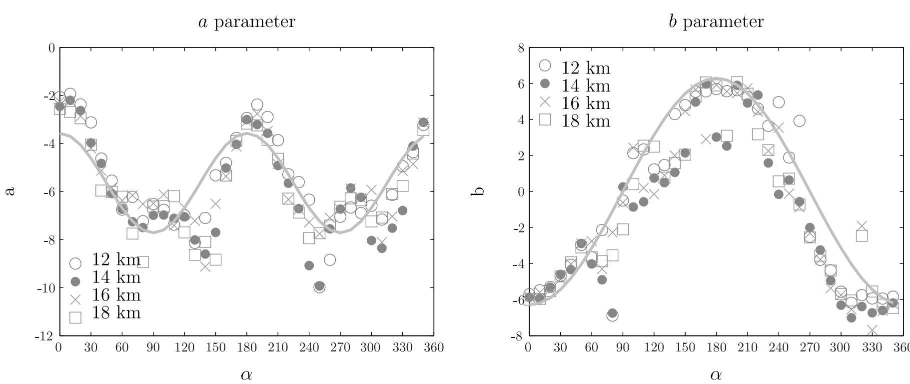

Fig. 10 a and b parameters as a function of α for wind speed for separation distances 12, 14, 16 and 18 km.

Based on the fitted curves, the two parameters have the forms:

$$a(\alpha) = 1.8cos(\frac{2\pi\alpha}{180}) - 5.9 \tag{16}$$

$$b(\alpha) = 2\pi cos(\frac{\pi\alpha}{180}) \tag{17}$$

and

$$\mathrm{Co_n}(\alpha, d, V_0, f) = e^{a(\alpha)\frac{fd}{V_0}} cos(b(\alpha)\frac{fd}{V_0}) \tag{18}$$

$$\mathrm{Qu_n}(\alpha, d, V_0, f) = e^{a(\alpha)\frac{fd}{V_0}} sin(b(\alpha)\frac{fd}{V_0}) \tag{19}$$

In other words, if the wind direction and wind speed are known for a pair of points separated by a distance d, then the co- and quadrature spectra can be estimated. The behaviour of the functions are demonstrated in figure 11, where α, d and V_0 are systematically varied.

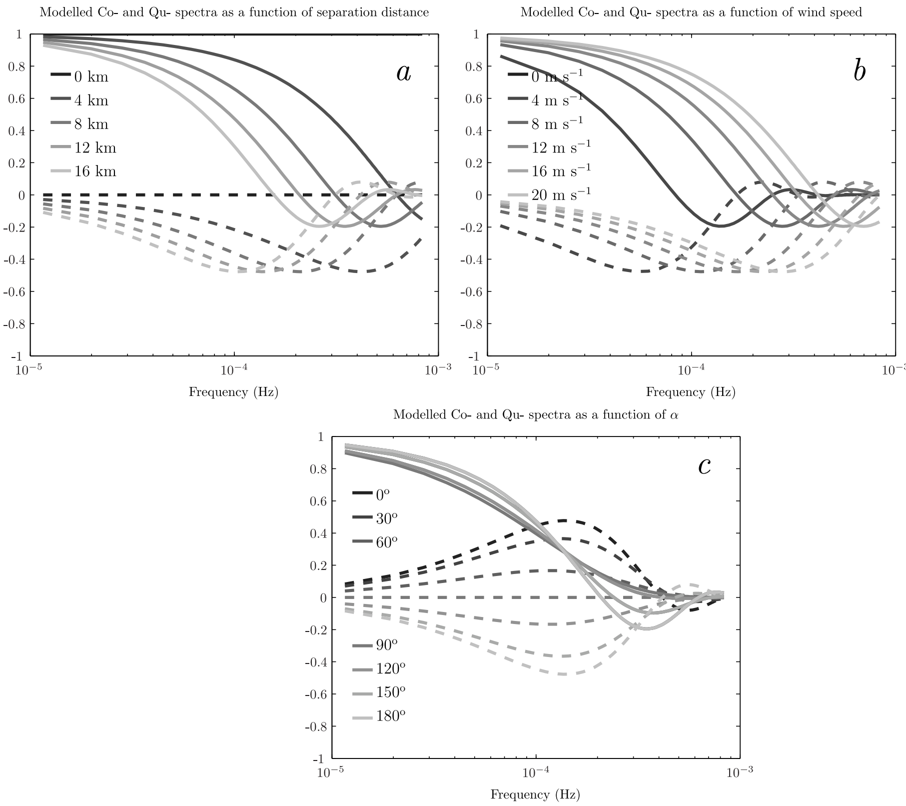

Fig. 11 (*a*) Normalized co- and quadrature- spectra as a function of separation distance for constant wind speed (12 m s^{-1}) and α (0 degrees). (*b*) Normalized co- and quadrature spectra as a function of wind speed for constant separation distance (10 km) and α (0 degrees). (*c*) Normalized co- and quadrature spectra as a function of α for constant wind speed (12 m s^{-1}) and separation distance (10 km).

Finally, the analytical models in equations 18 and 19 are fitted to two examples of observed flow from the sea for Horns Rev I and Nysted respectively. We choose conditions that are well represented in the data, and which are indicative of flow from the sea. The conditions for selection of the data, and the parameters used in equations 18 and 19 are described in table 2.

Table 2 Example conditions of flow from the sea for chosen for illustrating the models proposed in equations 18 and 19

Mast	α_{obs}	$V_{0,\mathrm{obs}}$ m s^{-1}	α_{model}	$V_{0,\mathrm{model}}$ m s^{-1}	d_{model} m
Horns Rev M2-M7	$> 337.5^{\mathrm{o}}$, $< 22.5^{\mathrm{o}}$	7–9	0^{o}	8	12420
Nysted M2-M3	$> 337.5^{\mathrm{o}}$, $< 22.5^{\mathrm{o}}$	7–9	0^{o}	8	8920

Figure 12 shows the modelled and observed spectra for the two sets of conditions described in Table 2. Both of the cases are representative of conditions over the sea, where the analytical model performs well. For flow that is more influenced by the land than the sea, the analytical models do not perform as well, and we expect that for conditions over land, the spectra are more difficult to relate to the simple advection and exponential decay terms that were used in deriving equations 18 and 19.

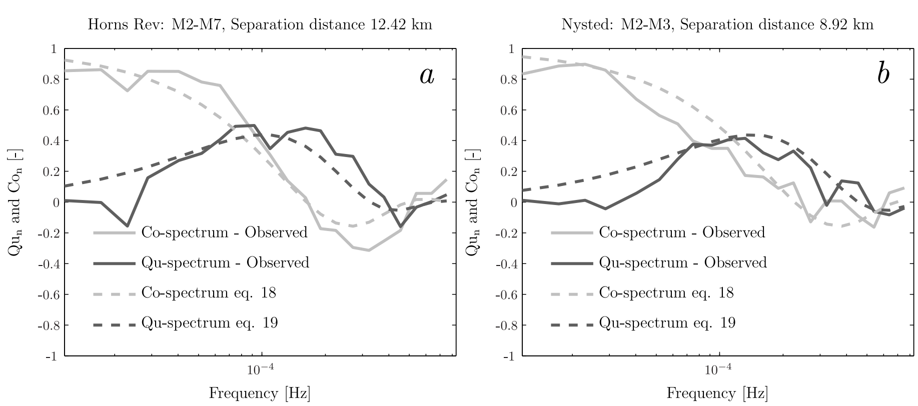

Fig. 12 Normalized co-spectra and quadrature spectra calculated from observations (solid lines) and from analytical models in equations 18 and 19 for the conditions described in table 2 at Horns Rev I (*a*) and Nysted (*b*).

6 Discussion

The normalized co-spectra and quadrature spectra for Horns Rev I and Nysted show the expected patterns with respect to the relative angle between the wind direction and the separation of the mast-pairs. For lateral flow, where there should not be any systematic phase shift at the two sites, the normalized quadrature spectrum is close to zero for all frequencies, while the normalized co-spectrum (in this case, equivalent to the coherence) decreases exponentially. For longitudinal flow, there is a systematic phase shift in the wind speed at the two sites as reflected in the peak in the normalized quadrature spectrum and zero-crossing in the normalized co-spectrum at a normalized frequency close to 0.25. The normalized frequency of 0.25 corresponds to eddies or structures that have a length scale 4 times the separation distance, which will bring about a phase shift of 90^{o}. Similarly, the normalized co-spectrum reaches a local minimum and the quadrature spectrum crosses the frequency axis at a normalized frequency of about 0.5, corresponding to eddies or structures with a length scale of twice the separation distance that will result in a phase shift of 180^{o} . Thus the normalized co-spectra and quadrature spectra form a pair of exponentially damped cosine and sine functions. The eddies or boundary layer structures corresponding to each frequency continue to cause in-phase or out-of-phase fluctuations at pairs of sites as the frequency increases, depending on the ratio between the length scale of the eddies and the distance between the sites. At the same time, as the eddies get smaller in relation to the distance between the sites, they are more likely to have undergone changes in their size or amplitude as they are advected between the sites, causing the coherence to decrease.

There was general agreement in the shape of the normalized co-spectra and quadrature spectra for Horns Rev I and Nysted, but there were important differences. At Nysted, the quadrature spectrum has the characteristic peak at a normalized frequency of 0.25 only for the longitudinal westerly case, and does not show any peak at all for the longitudinal easterly case, and the magnitude of the quadrature spectrum is larger at Horns Rev I than at Nysted. Similarly, the normalized co-spectra decrease to zero as expected for normalized frequencies of about 0.25 at Nysted, but do not pass far below the zero axis. This is likely to be due to the complex coastline at Nysted, which also affects the spectra calculated from the WRF simulation over the Baltic Sea - even though the grid points have been shifted southwards to avoid the land itself, the region is surrounded by coastlines. Also, different meteorological conditions exist over the North Sea and the Baltic Sea (Larsén et al, 2011b), and some of the differences may be attributable to the different boundary layer phenomena that dominate the near-surface wind conditions.

In the WRF model output, the patterns in the normalized co-spectra and quadrature spectra are somewhat better defined and easier to relate to the simplistic conceptual model of eddies of various sizes being advected past the pair of sites while simultaneously decaying or deforming. For example, the longitudinal normalized co-spectra from the model output dip further below zero than the observed longitudinal normalized co-spectra. Furthermore, the quadrature spectra from the model are nearly symmetrical about the horizontal axis for supplementary pairs of angles, while the peak in the observed quadrature spectrum is larger for flow from the sea than for flow from the land. There are several reasons for these differences. First, the model spectra are based on data that are further away from the land than the observed data, which means that the model spectra are less influenced by surface inhomogeneities. Secondly, the model is simpler than the real world, since there are no sub-grid scale processes. Real-world phenomena such as rain showers from individual cumulus clouds, entrainment at the top of the boundary layer and microscale turbulent eddies do not exist in the model, and it therefore seems more likely that mesoscale eddies that have length scales of tens of kilometres could be advected between the masts in a relatively undisturbed way.

The expressions in equations 18 and 19 were shown to be an excellent fit to the spectra from the WRF model output, which are representative of conditions over the sea. The expressions were also shown to be a good fit for the observed spectra from both Horns Rev I and Nysted for selected cases where the wind was blowing from the sea with a relatively uninterrupted sea fetch. The additional input of the mesoscale model thus made it possible to extend limited observational evidence to derive useful expressions for the shape of the normalized co-spectrum and quadrature spectrum over the sea, and to describe the underlying physics behind the shape of the spectra. Although the prohibitive computational costs of mesoscale models are often cited as problematic for such work, we found physically reasonable and robust results using wind speeds saved every 10 minutes from simulations of length 3 months, with a horizontal grid spacing of 2 km. The results suggest that mesoscale models could be used for conducting similar studies over land, although unresolved sub-grid-scale topographic effects might have serious consequences at some sites.

The decay factors, $a(\alpha)$, in equations 18 and 19 are 4.1 and 7.7 for longitudinal and lateral flow respectively. These values can be compared, to some extent, to the decay factors in Schlez and Infield (1998). For separation distances between 62 and 102 m and a sampling frequency of 0.2 Hz, they suggest decay factors of $15\sigma/V_0$ for longitudinal flow, and 17.5σ for lateral flow, where σ is the standard deviation of the time series. Applying the expressions to our time series, which are longer and consist of ten minute averages, is problematic due to the sensitivity of the standard deviation to the averaging and sampling frequency. However, with a nominal wind speed of 10 m s^{-1} and a standard deviation of around 1 m s^{-1}, the expressions of Schlez and Infield (1998) give decay factors of 1.5 and 17.5 for longitudinal and lateral flow respectively. Sørensen et al (2008) proposed the values 4 and $V_0/2$ (5 for a nominal wind speed of 10 m s^{-1}) for the longitudinal and lateral decay factors in the expressions of Schlez and Infield (1998) based on measurements separated by between 300 m and 1200 m at a flat coastal site in Denmark. The values found in this paper are quite close to those suggested by Sørensen et al (2008), despite the fact that they are calculated for separation distances of 12–18 km and for conditions over the sea.

The calculation of normalized co-spectra and quadrature spectra is actually a useful model verification tool, since it is insensitive to errors in the phase of high frequency fluctuations in the model with respect to the observed fluctuations, which are not possible to forecast in a deterministic sense. Instead, it addresses the amplitude and spatial patterns in the fluctuations. The results presented here show good agreement between modelled and observed spectra for time scales up to 20 minutes, and spatial scales up to 12 km for average, near-stationary conditions. On the other hand, the precise spectral performance of the model in terms of simulating the spatial covariance during special meteorological conditions or topographically driven phenomena depends on whether the model is able to accurately reproduce the physical processes and the correct length scales associated with the conditions, and this is an open area for further investigation.

The results are climatological averages that include several years of observations, or 3 months of model data. Obviously many and varied physical processes are contained within the reasonable stationary and homogeneous situations that were identified according to the stationarity criteria. The general spectral shapes that were calculated therefore incorporate various dynamic and convective processes for unstable conditions, and turbulence and gravity wave processes for stable conditions. For example, Larsén et al (2011b) demonstrated that the co-spectrum and quadrature spectrum for 24 hour periods where open cellular convection was observed over the North Sea appear to show both a larger peak in the quadrature spectrum and a deeper trough below zero in the co-spectrum than cases where cellular convection was not observed. In stable conditions, gravity waves also affect the spectral properties of the wind speed, as demonstrated in Larsén et al (2011a,b). The shape of the spectra under specific meteorological conditions is an important area for further study, although finding sufficient data from pairs of tall masts under a narrowly defined set of conditions makes this difficult. Furthermore, by filtering out cases where there was a large wind speed or direction change, many situations that are of great scientific and practical interest have actually been excluded from this analysis. In particular, large changes in wind speed (often referred to as 'ramp events' in a wind energy context (Potter et al, 2009)) and the way they propagate through wind farms or groups of wind farms are of obvious relevance to wind energy control and integration.

The normalized co-spectra and quadrature spectra presented here are based on the scalar wind speed, despite the fact that cross-spectral analysis of wind time series on microscales is traditionally separated into u (along wind) and v (across wind) components (eg. Kristensen (1979); Kristensen and Jensen (1979)). Decomposition into u and v components is considerably more difficult for mesoscale time scales, where the wind direction is rarely even nearly constant for a 24 hour period, and fluctuations in wind direction can have a disproportionately large impact on the v wind component. Although the decomposition could be achieved with a very strict set of filtering criteria for wind direction, we restricted the analysis to the scalar wind speed. Careful analysis of the spectral and cross-spectral properties of u and v wind components, as performed in Larsén et al (2011b), can reveal important results about the isotropy of the wind field.

The results in this paper focused on conditions over the sea. However, it was implied that conditions may not be the same over the land as over the sea. For example, the shape of the quadrature spectrum for Horns Rev I was less pronounced for easterly sector winds than for westerly sector winds, and the quadrature spectrum for Nysted (which is closer to coastlines from all directions) did not show the clear or systematic patterns that were seen for Horns Rev I. Woods et al (2011) found that the advection speed of wind fluctuations was only weakly related to the mean wind speed for pairs of near-surface meteorological masts over the land, which might reflect the stronger impact of local features over the land in modulating the surface wind conditions compared to the relatively homogeneous conditions over the sea. That is, the application of Taylor's hypothesis for mesoscale wind fluctuations is likely to be more straightforward over the sea than over the land. Meteorological conditions over the sea are different to conditions over the land due to the low surface roughness, the absence of topographic effects, the ample supply of moisture and the stability conditions driven by advection of air masses rather than the radiation balance. Such differences can influence the spectral properties of the wind speed, particularly in the mesoscale range. For example, organized mesoscale structures such as cellular convection, convective rolls or gravity waves may have a strong influence on the mesoscale wind speed over the sea. These differences are important for the planning and operation of offshore wind energy, where the spatial correlation in wind speeds at a certain frequency can undermine the potential for smoothing of the aggregated power output from spatially distributed turbines.

7 Conclusions

Normalized co-spectra and quadrature spectra were calculated using 10 min wind speed observations from pairs of offshore meteorological masts over the North Sea and the Baltic Sea respectively. Separation distances between the masts ranged from 2.13 km to 12.4 km, and results were binned according to the relative direction between the mean wind and the orientation of the mast pairs. Co-spectra and quadrature spectra were also calculated using 3 month mesoscale model simulations over the North Sea and the Baltic Sea, and good agreement was found between the observed and modelled spectra when the flow was coming from the sea.

For flow over the sea, the co-spectrum and quadrature spectrum could be effectively modelled using damped cosine and sine functions based on a constant delay time associated with advection between the two sites. The simple analytical models were found to be an excellent fit to the spectra derived from mesoscale modelling over the sea, and for observed spectra where the flow had a long sea fetch. For flow that did not have a long sea fetch, the patterns in the spectra were less clear, although there was still a greater contribution to the quadrature spectrum for longitudinal flow than for lateral flow. The extent to which the analysis presented here for flow over the sea could be extended or adapted to flow over a relatively homogeneous land area has not been tested.

The results are unique because they are based on pairs of tall offshore measurement masts, which are much less common than onshore measurement masts. The situation of Horns Rev I, with a long sea fetch to the west, and a North-South coastline to the east, provided a particularly simple and useful analysis site. Furthermore, the use of the WRF model to expand the scope of the observation analysis was a useful and novel application of mesoscale modelling.

Like most spectral analysis of geophysical time series, the results were limited by the assumptions of stationarity. This meant that many interesting meteorological cases were not included in the analysis, because they contained large changes in wind speed or wind direction. The precise impacts of the wind farm wakes, and of different classes of synoptic and mesoscale conditions on the spectra are interesting areas for future work.

Acknowledgements The contribution of C.L. Vincent was supported by the Danish Council for Independent Research – Technology and Production Sciences (case number 10-093196) individual post-doc project. The contribution of the remaining authors was supported by the Danish project 'Mesoscale variability and the variability of wind and production of offshore wind farms (contract number PSO-1741). The authors are grateful to Dong Energy and Vattenfall for permission to use observational data from the Horns Rev I and Nysted wind farms.

References

Davenport AG (1961) The spectrum of horizontal gustiness near the ground in high winds. Quart J Roy Meteor Soc 87:194–211

Davies-Jones R (2002) Linear and nonlinear propagation of supercell storms. J Atmos Sci 59:3178–3205

Gage KS, Nastrom GD (1986) Theoretical interpretation of atmospheric wavenumber spectra of wind and temperature observed by commercial aircraft during GASP. J Atmos Sci 43:729–740

Kain JS, Fritsch JM (1990) A one-dimensional entraining/detraining plume model and its application in convective parametrization. J Atmos Sci 47:2784–2802

Kristensen L (1979) On longitudinal spectral coherence. Bound Layer Meteorol 16:145–163

Kristensen L, Jensen NO (1979) Lateral coherence in isotropic turbulence and in the natural wind. Bound Layer Meteorol 17:353–373

Kristensen L, Kirkegaard P (1986) Sampling problems with spectral coherence. Risø report Risø-R-526, Risø National Laboratory, Roskilde, Denmark

Larsen GC, Mann J, Ighil TA, Mouritzen AS (2009) Do wind farms influence large scale turbulence? Extended Abstracts for Euromech Colloquium 508, pp 38–40

Larsén XG, Larsen S, Badger M (2011a) A case-study of mesoscale spectra of wind and temperature, observed and simulated. Quart J Roy Meteor Soc 137:264–274

Larsén XG, Vincent CL, Larsen SE (2011b) Spectral structure of the mesoscale winds over the water. Quart J Roy Meteor Soc. Manuscript under revision

Madsen H (2008) Time Series Analysis. Chapman & Hall, London

Molinari J, Dudek M (1992) Parametrization of convective precipitation in mesoscale numerical models: a critical review. Mon Wea Rev 120:326–344

Nakanishi M, Niino H (2009) Development of an improved turbulence closure model for the atmospheric boundary layer. J Meteor Soc Japan 87:895–912

Nanahara T, Asari M, Sato T, Yamaguchi K, Shibata M, Maejima T (2004) Smoothing effects of distributed wind turbines. Part 1. coherence and smoothing effects at a wind farm. Wind Energy 7:61–74, DUI 10.1002/we.109

Nastrom GD, Gage KS (1985) A climatology of atmospheric wavenumber spectra of wind and temperature observed by commercial aircraft. J Atmos Sci 42:950–960

Potter CW, Grimit E, Nijssen B (2009) Potential benefits of a dedicated probabilistic rapid ramp event forecast tool. In: IEEE/PES power systems conference and exposition, vol 1-3, pp 409–413

Schlez W, Infield D (1998) Horizontal, two point coherence for separations greater than the measurement height. Bound Layer Meteorol 87:459–480

Sioutas MV, Flocas HA (1996) Influence of environmental winds on propagation and motion of thunderstorms in northern Greece. J Geophys Res 101:26,255–26,265

Skamarock WC (2004) Evaluating mesoscale NWP models using kinetic energy spectra. Mon Wea Rev 132:3019–3032

Skamarock WC, Klemp JB, Dudhia J, Gill DO, Barker DM, Duda MG, Huang XY, Wang W, Powers JG (2008) A description of the advanced research WRF version 3. NCAR Technical Note TN-475+STR, NCAR, Boulder, Colorado

Sørensen P, Hansen AD, Rosas PAC (2002) Wind models for simulation of power fluctuations from wind farms. J Wind Eng Ind Aerodyn 90:1381–1402

Sørensen P, Cutululis NA, Vigueras-Rodríguez A, Madsen H, Pinson P, Jensen L, Hjerrild J, Donovan M (2008) Modelling of power fluctuations from large offshore wind farms. Wind Energy 11:29–43

Troldborg N, Larsen GC, Madsen HM, Hansen KS, Sørensen JN, Mikkelsen R (2011) Numerical simulations of wake interaction between two wind turbines at various inflow conditions. Wind Energy 14:859–876

Vigueras-Rodrìguez A, Sørensen P, Cutululis NA, Viedma A, Donovan MH (2010) Wind model for low frequency power fluctuations in offshore wind farms. Wind Energy 13:471–482, DUI 10.1002/we.368

Woods JW, Davy RJ, Russell CJ, Coppin PA (2011) Cross-spectrum of wind speed for meso-gamma scales in the upper surface layer over South-Eastern Australia. Bound Layer Meteorol 141:93–116, DOI: 10.1007/s10546-011-9632-2